Int. J. Heat Mass Transfer. Vol. 27, No. 2, pp. 207–219, 1984
Printed in Great Britain

0017–9310/84 $3.00 + 0.00

NATURAL CONVECTION IN A VERTICAL POROUS ANNULUS

V. PRASAD and F. A. KULACKI†
Department of Mechanical and Aerospace Engineering, University of Delaware, Newark, DE 19711, U.S.A.

(*Received* 29 *September* 1982 *and in revised form* 23 *May* 1983)

Abstract—Numerical studies are reported for steady free convection in a vertical annulus filled with a saturated porous medium and whose vertical walls are at constant temperatures, the horizontal walls being insulated. Curvature effects on temperature and velocity fields are significant, and completely disturb the centro-symmetrical nature found in the vertical cavity case. Convective velocities are higher in the upper half than the lower half of the annulus, and the local rate of heat transfer is much higher near the top edge of the cold wall. The average Nusselt number always increases as the radius ratio, κ, increases, though the rate of increase diminishes with the increase in curvature effects particularly at high Rayleigh numbers, Ra*. In the case of a tall annulus the heat transfer rate in the boundary layer flow regime approaches that for a cylinder embedded in a porous medium, as κ increases. The Rayleigh number criteria for various flow regimes are obtained, and the average Nusselt number is correlated by a relation of the form $Nu = \text{const.}\ Ra^{*m} A^{n} \kappa^{p}$, where A is the aspect (height-to-gap width) ratio. In the boundary layer regime, the heat transfer rate for a tall cavity or annulus of fixed height is a very weak function of the aspect ratio.

NOMENCLATURE

A	aspect ratio, L/D
c	specific heat of fluid at constant pressure [J kg^{-1} K^{-1}]
C	constant for equation (27)
D	gap width of porous annulus, $r_o - r_i$ [m]
g	acceleration due to gravity [m s^{-2}]
$\bar{g}$	body force vector [m s^{-2}]
h	heat transfer coefficient [W m^{-2} K^{-1}]
$\bar{h}$	average heat transfer coefficient on vertical wall [W m^{-2} K^{-1}]
K	permeability of porous medium [m^2]
k_m	effective thermal conductivity of the saturated porous medium [W m^{-1} K^{-1}]
L	height of porous annulus [m]
Nu_z	local Nusselt number on heated wall, hz/k_m
Nu	average Nusselt number, $\bar{h}D/k_m$
p	pressure [Pa]
Pr	Prandtl number, ν/α
Ra^*	Rayleigh number, $(g\beta K D \Delta T)/(\nu\alpha)$
T	temperature [K]
ΔT	temperature difference across annulus, $T_i - T_o$ [K]
u	fluid velocity in r-direction, $-(\alpha/D)\,[1/(\gamma R+1)]\,(\partial\psi/\partial Z)$
v	fluid velocity in z-direction, $(\alpha L/D^2)[1/(\gamma R+1)](\partial\psi/\partial R)$
$\bar{V}$	velocity vector [m s^{-1}]
r, z	cylindrical coordinates [m]
R	dimensionless distance on r-axis, $(r-r_i)/D$
Z	dimensionless distance on z-axis, z/L.

Greek symbols

α	thermal diffusivity of porous medium, $k_m/\rho c$ [m^2 s^{-1}]
β	isobaric coefficient of thermal expansion of fluid [K^{-1}]
γ	radius ratio parameter, $D/r_i = \kappa - 1$
η	inverse of radius ratio, $1/\kappa = r_i/r_o$
θ	dimensionless temperature, $(T-T_o)/(T_i-T_o)$
κ	radius ratio, r_o/r_i
μ	dynamic viscosity of fluid [kg m^{-1} s^{-1}]
ν	kinematic viscosity of fluid [m^2 s^{-1}]
ρ	density of fluid [kg m^{-3}]
ψ'	stream function
ψ	dimensionless stream function, $(D/\alpha r_i L)\psi'$.

Subscripts

cond	conduction
i	inner wall (heated)
L	based upon annulus height, L
o	outer wall (cooled)
r	reference point for equation (5)
r_o	based upon outer radius, r_o
w	wall
z	local value on vertical wall.

1. INTRODUCTION

INTEREST in understanding the convective transport processes in porous materials is increasing owing to the development of geothermal energy technology, high performance insulation for building and cold storage, renewed interest in the energy efficient drying processes, and many other areas. A few other technological applications of natural convection in a porous medium are cooling of nuclear fuel in shipping flasks and water filled storage bays, insulation of high temperature gas cooled reactor vessels, burying of drums containing heat generating chemicals in the earth, thermal energy storage tanks, regenerative heat exchangers containing porous materials, petroleum reservoirs, and chemical catalytic reactors. Combarnous and Bories [1], Cheng [2] and Combarnous [3], have recently provided extensive reviews of state-of-the-art on free convection in fluid-saturated porous media.

† Author to whom correspondence should be addressed.

Natural convection in differentially heated vertical enclosures is of fundamental interest to many practical applications. Several investigators have presented analytical and experimental results for the rectangular cavity with vertical walls at constant temperatures, the horizontal walls being insulated [4–16]. Analytical work includes numerical solutions, boundary layer solutions, integral analyses and series solutions. Based on these studies, various correlations have been presented for average heat transfer coefficients, and these cover a wide range of Rayleigh numbers and aspect ratios [4, 8, 10, 12]. Recently, Prasad and Kulacki [17] have reported numerical results for the case when a constant heat flux is applied on one vertical wall, and the other vertical wall is isothermally cooled.

In spite of the importance of convective heat transfer results for the vertical annular enclosures filled with saturated porous media, to practical applications, there was nothing available in the literature until very recently. The present available reports are due to Hickox and Gartling [18], and Havstad and Burns [19]. Hickox and Gartling [18] have considered a case when the inner wall is heated at a constant temperature and the outer wall is isothermally cooled, the top and bottom being insulated. Using a finite element technique, they have obtained heat transfer results for Rayleigh numbers, Ra^*, up to 100. The ranges of the aspect ratio considered are $2 \leqslant A \leqslant 8$, and $2 \leqslant L/r_i = A(\kappa-1) \leqslant 8$, respectively. Following an approach utilized by Burns *et al.* [11], which was based upon Batchelor's work [20], they have also developed an approximate analytical method valid for low Rayleigh numbers and high aspect ratios.

Havstad and Burns [19] have used three different methods, finite-difference numerical method, an approximate analysis and the perturbation technique to analyse the problem. Out of these, only the first two have been used to obtain heat transfer results whereas the perturbation technique is used only to establish temperature and velocity fields for very low Rayleigh numbers. The approximate analysis is again based upon the previous works [11, 20]. Though most of the results obtained by Havstad and Burns [19] are for the same thermal boundary conditions as considered by Hickox and Gartling [18], the authors [19] have also presented the effect of the wall Biot number when the heat is rejected to the ambient through a conducting wall. The results presented by Havstad and Burns [19] are in terms of a Rayleigh number based on the outer radius, $Ra^*_{r_o}$, the height-to-outer radius ratio, L/r_o, and the radius ratio, r_i/r_o, for the range of $35 \leqslant Ra^*[\kappa/(\kappa-1)] \leqslant 150$, $0.5 \leqslant A[(\kappa-1)/\kappa] \leqslant 20$ and $1 \leqslant \kappa \leqslant 10$ in terms of the parameters used in the present work. To analyze the temperature and flow fields, both the studies [18, 19] present some representative streamlines and isotherm patterns.

Though the work of Hickox and Gartling [18], and of Havstad and Burns [19] present interesting and useful results for the annulus problem, their studies consider a limited range of Rayleigh numbers, and as such, are restricted to the conduction and the asymptotic flow regimes. The purpose of the present work is to consider the problem for a relatively wide range of Rayleigh numbers, Ra^* up to 10000 and to study the boundary layer and curvature effects in the presence of strong convective flows. Consequently, in the present analysis the aspect (height-to-gap width) ratio, A, varies between 1 and 20 for a radius range of $1 \leqslant \kappa \leqslant 26$. The flow patterns and isotherms exhibit a significant influence of curvature. Though the effects of the Rayleigh number and the aspect ratio are qualitatively similar to what has been observed for the vertical cavity, the correlations for the average Nusselt number require modification to include the curvature effects. Expressions for critical Rayleigh number have also been obtained to delimit the various flow regimes.

2. FORMULATION

Based on Darcy's law, the governing equations for steady, free convection in a homogeneous, isotropic porous medium are [1]

$$\nabla \cdot \bar{V} = 0, \tag{1}$$

$$-\nabla p + \rho \bar{g} - \frac{\mu}{k}\bar{V} = 0, \tag{2}$$

$$\rho c(\bar{V} \cdot \nabla)T = k_m \nabla^2 T, \tag{3}$$

$$\rho = \rho_r[1 - \beta(T - T_r)]. \tag{4}$$

These equations are based on the assumptions that the fluid properties are constant, except for the density variation in producing the buoyancy force. Additional viscous drag (Brinkman model) and inertia terms are neglected because their order of magnitudes are small compared to other terms for low Darcy numbers. Thus, velocity slip at the walls is permitted. Dispersion effects are also neglected in the present formulation.

For axisymmetric flow, equations (1)–(3) may be written as

$$\frac{\partial(ru)}{\partial r} + \frac{\partial(rv)}{\partial z} = 0, \tag{5}$$

$$\frac{\partial p}{\partial r} + \frac{\mu}{K}u = 0, \tag{6}$$

$$\frac{\partial p}{\partial z} + \rho g + \frac{\mu}{K}v = 0, \tag{7}$$

$$u\frac{\partial T}{\partial r} + v\frac{\partial T}{\partial z} = \alpha\left[\frac{1}{r}\frac{\partial}{\partial r}\left(r\frac{\partial T}{\partial r}\right) + \frac{\partial^2 T}{\partial z^2}\right]. \tag{8}$$

Defining stream function, ψ', as

$$u = -\frac{1}{r}\frac{\partial \psi'}{\partial z}, \tag{9}$$

and

$$v = \frac{1}{r}\frac{\partial \psi'}{\partial r}, \tag{10}$$

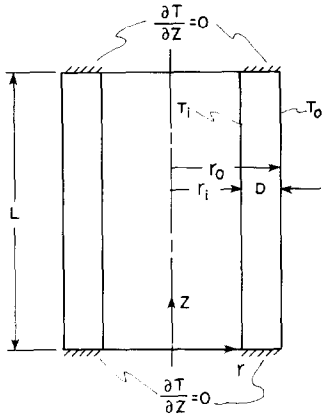

FIG. 1. Vertical annulus, coordinate system, and thermal boundary conditions ($T_i > T_o$).

and using dimensionless variables, equations (5)–(8) and equation (4) reduce to the stream function form

$$A^2 \frac{\partial}{\partial R}\left[\frac{1}{(\gamma R+1)}\frac{\partial \psi}{\partial R}\right] + \frac{\partial}{\partial Z}\left[\frac{1}{(\gamma R+1)}\frac{\partial \psi}{\partial Z}\right] = Ra^* A \frac{\partial \theta}{\partial R}, \quad (11)$$

$$\frac{\partial \psi}{\partial R}\frac{\partial \theta}{\partial Z} - \frac{\partial \psi}{\partial Z}\frac{\partial \theta}{\partial R} = \frac{\partial}{\partial R}\left[(\gamma R+1)\frac{\partial \theta}{\partial R}\right] + \frac{1}{A^2}\frac{\partial}{\partial Z}\left[(\gamma R+1)\frac{\partial \theta}{\partial Z}\right]. \quad (12)$$

The relevant hydrodynamic boundary conditions for no mass flux through the boundaries and the thermal boundary conditions are (Fig. 1)

$$\psi = 0, \quad \theta = 1 \quad \text{at} \quad R = 0, \quad (13)$$

$$\psi = 0, \quad \theta = 0 \quad \text{at} \quad R = 1, \quad (14)$$

$$\psi = 0, \quad \frac{\partial \theta}{\partial Z} = 0 \quad \text{at} \quad Z = 0 \quad \text{and} \quad 1. \quad (15)$$

It may be noted that the present approach of formulating the problem and introducing the dimensionless parameters reduces the present problem to an extension of the rectangular cavity case. Equations (11) and (12), hence, can be readily converted to those for a rectangular coordinate system, just by substituting $\gamma = 0$ (for cavity).

3. NUMERICAL METHOD

Equations (11) and (12) are transformed into difference equations by using a finite-difference scheme, for axisymmetric recirculating flows, developed by Gosman *et al.* [21] and recently applied to natural convection problems by several investigators. The method has been found not to suffer with the drawbacks of less accuracy and/or large computational time at reasonably high Rayleigh numbers. Also, it has been possible to use it for large radius ratios, e.g. $\gamma = 25$, even at high values of Ra^*.

In the present scheme, finite-difference equations† are obtained by integrating the governing differential equations over finite area elements, instead of using a Taylor's series expansion. This approach ensures that the conservation laws are obeyed over arbitrarily large or small portions of the domain, and experience so far has indicated that conservative systems do generally give more accurate results [21, 22].

A grid is established by dividing the region in R and Z directions. A micro-cell is then considered around each nodal point through half-distance points [21]. Equations (11) and (12) are then integrated over each cell as proposed by Gosman *et al.* [21]. This introduces upwind differences for the convective terms in the energy equation and is equivalent to second upwind differencing [22]. The successive substitution formulae derived in this way satisfy the convergence criterion and is quite stable for many circumstances [21]. For solving the system of algebraic equations thus obtained, the Gauss–Seidel method is used which makes use of the new values as soon as they are available.

To be consistant with the integral formulation for the system, boundary conditions for the specified temperature gradients are applied using two-point formula for the derivative. The use of the Taylor's series up to third-order terms to fix the gradient does not bring any appreciable change in the results, though the number of iterations required for the convergence is slightly reduced. This may be due to the monotonic change in the temperature and the small grid sizes being used near the walls. For evaluating the derivatives at any point inside the domain (at a central point), two neighboring points are always taken into consideration.

To test the applicability and accuracy of the present method, results were obtained for the vertical cavity case, $\gamma = 0$, and were compared with the existing results. Various combinations of uniform and non-uniform grid fields were used to select one which would yield good accuracy and yet require less computational time. It was observed that the use of varying grids with fine mesh near the walls is advantageous and more reasonable owing to boundary layers on the vertical walls and significant changes in the magnitude and direction of velocities near the horizontal walls. A 21 × 21 non-uniform mesh was found to be a reasonably good choice for the vertical cavity case for low aspect ratio ($A < 5$). For high aspect ratio, the proper grid size varied between 11 × 15 to 15 × 21 depending upon the Rayleigh number. When computations were made for the annulus, it was observed that to get the same accuracy the number of grids must be increased. The worst case is when both γ and Ra^* are large. For the present results, as γ and Ra^* increase, the number of grid sizes have been increased, and as such, for $A = 1$, it varies between 21 × 21 to 31 × 31.

† For derivation of the finite-difference equations the divergence form of equations (3) and (12) is used.

For higher aspect ratios, the number of grids in the z-direction is taken up to 41. In each case, varying grids were used in both r- and z-directions for $Ra^* \geqslant 200$, whereas for lower Rayleigh numbers uniform grids were employed. For the trial cases, the selected mesh sizes gave an average Nusselt number within 2% of the asymptotic value predicted by calculations with much finer grids when Ra^* and γ are not very large. For high Rayleigh numbers, $Ra^* \geqslant 2000$ and high radius ratios, $\gamma \geqslant 10$, a variation of 3% was accepted to keep the CPU time low.

For low Rayleigh numbers over-relaxation of the temperature helped in obtaining faster convergence, and for high Rayleigh numbers under-relaxation of the stream function was found useful. The over-relaxation parameter used was as high as 1.9 for $Ra^* < 50$ and was varied between 1.9 and 1, whereas a suitable value for the under-relaxation parameter was between 0.5 and 1.

To judge the iterative convergence of the solution a criterion

$$\left[1 - \frac{\phi^{n-1}}{\phi^n}\right]_{\max} < \varepsilon, \tag{16}$$

was used at each point in the domain for both the temperature, θ, and the stream function, ψ. To establish a proper value of ε, computations were done with several combinations of Ra^*, A and γ, for ε varying between 10^{-3}–10^{-5}. The maximum change in the Nusselt number was up to 1%, whereas in many cases, the number of iterations required with $\varepsilon = 10^{-5}$ was about 1.5 times that needed for $\varepsilon = 10^{-3}$. To keep the computational costs low, a suitable value for ε was taken as 0.0005, which provided a convergence accuracy of 0.25%.

To have an additional check on the accuracy of the results, an energy balance was used for the system. For this the heat transfer at $r = r_o$ is compared with the input at $r = r_i$. For 65% of the results reported here, the energy balance was satisfied to within 1%, whereas for the rest, it was within 5%. The worst cases were when the radius ratio was large, $\gamma \geqslant 10$, and the Rayleigh number was either very high, $Ra^* \geqslant 2000$, or very low, $Ra^* \leqslant 50$. A detailed discussion on the effects of upwind differencing, mesh sizes, relaxation parameters, convergence criterion etc. on the accuracy and the computational time are presented in ref. [16].

4. RESULTS AND DISCUSSION

4.1. *Temperature and velocity fields*

Results obtained for a wide range of Rayleigh numbers, $Ra^* \leqslant 10^4$, aspect ratios, $1 \leqslant A \leqslant 20$ and radius ratios $\kappa \leqslant 26$, show a distinct effect of curvature on the convective heat transfer. Flow patterns and temperature fields for some typical values of Ra^*, A and κ are presented in Figs. 2 and 3. It is observed that as the radius ratio increases, isotherms shift towards the inner (hot) wall. (See Figs. 2(a) and (b); also compare with the plots given in refs. [5, 9, 16].) The shift is more pronounced as the Rayleigh number and/or the aspect ratio increase. This results in the asymmetry of the temperature field in the core. It can also be seen that as κ increases, the change in temperature with respect to height, reduces in the lower half of the annulus, but increases faster in the upper half. Furthermore, the temperature gradient near the hot wall increases rapidly as the radius ratio increases. The behavior is just the reverse near the cold wall. A similar shift in isotherms toward the top of the cold wall has also been reported by Hickox and Gartling [18], and Havstad and Burns [19] for $\kappa = 1.67$ and 5, respectively. For a given aspect and radius ratio, an increase in Ra^* results in a thicker cold layer near the bottom wall and a high temperature field near the top wall [Figs. 2(b) and (c)].

A similar change in the temperature field with aspect and radius ratio has been reported by de Vahl Davis and Thomas [23, 24] and Lee *et al.* [25] for a vertical annulus filled with a Newtonian fluid, though no adverse temperature gradients or 'S-shaped' isotherms are observed in the present case. This is mainly due to the stronger conductive effects in the porous media [15].

The above change in the temperature field brings a noticeable change in the flow patterns as compared to those in a vertical cavity [5, 9, 16]. The growth of the boundary layers on the vertical walls are also observed to be affected by a variation in A and κ. The increase in radius ratio is seen to reduce the rate of boundary layer growth on the hot wall and is more prominent for the tall annulus (Fig. 3). This behavior is reversed on the cold wall. The net result is a shift of the core toward the top edge of the cooled wall. This shift is further strengthened if there is an increase in Ra^* and/or A. Generally higher convective velocities in the top right-hand corner are produced as a result of the shift. Also, the horizontal velocity in the upper region is much higher as compared to that in the lower region for increased values of A and/or κ. In short, the centro-symmetric property for the vertical cavity [10] is not found in the present case.

This shift of the core toward the top edge of the cold wall can also be visualized from the streamlines presented by Havstad and Burns [19], and Hilcox and Gartling [18]. The values of Ra^*, A and κ to present the streamlines and isotherms (Figs. 2 and 3) have been selected in such a way that they clearly demonstrate the effects of all three parameters, and compliments the information available for the temperature and flow fields [18, 19]. It may be noted that this general behavior of the core-region flow is qualitatively very similar to free convective flows for Newtonian fluids [23–25] though no multi-cellular flow is observed in the present case.

The temperature distributions at mid-height, $Z = 0.5$, are presented in Fig. 4 for $A = 1$ and 5, and $Ra^* = 1000$. As discussed earlier, an increase in radius ratio, introduces a decrease in temperature much faster near the hot wall and much slower near the cold wall. This

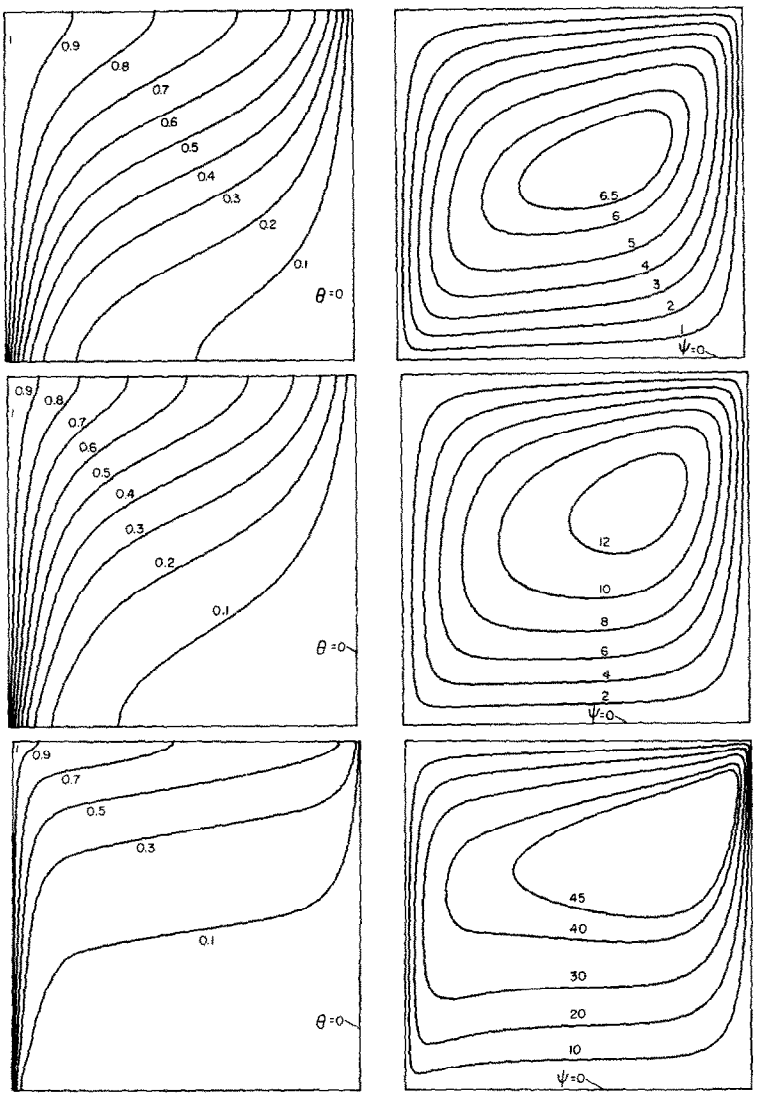

FIG. 2. Streamlines and isotherms for: (a) $Ra^* = 100$, $A = 1$ and $\kappa = 2$; (b) $Ra^* = 100$, $A = 1$ and $\kappa = 6$; and (c) $Ra^* = 1000$, $A = 1$ and $\kappa = 6$ (from top to bottom).

further indicates that the sink temperature for the boundary layer on the hot wall reduces as the curvature effects increase. Also, for high radius ratios, the conduction in the core is very small for any given Ra^* and A.

4.2. *Local heat transfer rate*

The local Nusselt number on the vertical wall in terms of the temperature difference, $T_i - T_o$, is given by

$$Nu_z = -AZ \left.\frac{\partial\theta}{\partial R}\right|_w. \tag{17}$$

Values of Nu_z are plotted in Figs. 5(a) and (b) for the inner and outer walls, respectively. It can be seen that the local Nusselt number on the heated wall first increases and then drops near the top wall [Fig. 5(a)]. This rate of increase and decrease are always higher for large κ and/or large A, though in each case, the heat transfer rate always decreases as Z increases, except for a very small distance (depending on the values of A and κ) from the lower edge. The decrease is slower in the lower portion, but much faster in the upper region. This behavior is a result of the reduced growth of the boundary layer for increased A and/or κ, and also, because of the change in the direction of flow taking place near the bottom edge. On the cold wall, the case is reversed. The rate of heat transfer is very high near the top edge [Fig. 5(b)], indicating that a large percentage of heat is being rejected in a very small distance from the top. For higher aspect ratios and/or lower radius ratios, the heat transfer is further enhanced near the top edge.

4.3. *Heat transfer results and criteria for flow regimes*

Based upon the annulus gap, D, the average Nusselt numbers on the inner and outer walls are given respectively by

$$Nu_i = -\int_0^1 \left.\frac{\partial\theta}{\partial R}\right|_{R=0} dZ, \tag{18}$$

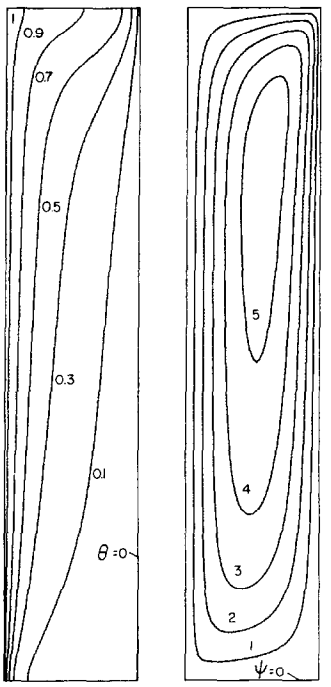

FIG. 3. Streamlines and isotherms for $Ra^* = 10^2$, $A = 5$ and $\kappa = 6$.

and

$$Nu_o = \kappa\, Nu_i. \tag{19}$$

Values of Nu_i are presented for a wide range of Ra^*, A and κ in Figs. 6–9. More results are reported in ref. [16].

Introduction of curvature effects ($\kappa > 1$) increases the Nusselt number on the inner wall. This is mainly due to the modification of temperature and velocity fields in the medium. The boundary layer temperature profiles are strongly affected and a lower sink temperature for the inner boundary layer results as the radius ratio is increased (Fig. 4). The rate of change in Nu_i is high at low values of Ra^* and is less for high Ra^* (Figs. 6–9).

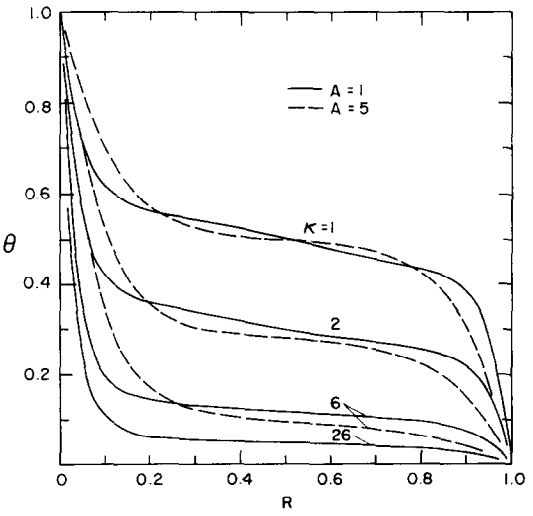

FIG. 4. Temperature distribution at mid-height of annulus ($Z = 0.5$) for $Ra^* = 10^3$.

In each case the Nusselt number approaches the asymptotic value

$$(Nu_i)_{cond} = \frac{(\kappa - 1)}{\ln(\kappa)}, \quad \kappa > 1, \tag{20}$$

and unity for the cavity, in the conduction regime. As usual, this conduction regime is always followed by the asymptotic and then by the boundary layer flow regimes [15]. It is observed that the conduction and asymptotic flow regimes get extended (in terms of Ra^*) as the radius ratio increases. The extension of the Rayleigh number range for the conduction regime is much more compared to that for the asymptotic flow regime. Consequently, the boundary layer flow is delayed as the curvature effects are increased. Following an approach presented in ref. [15] by the present authors, the criteria for different flow regimes in a tall annulus ($A > 2$) are obtained as

$$Ra^* > 4.8A^{0.73}\kappa^{0.40}, \quad \text{for asymptotic flow,} \tag{21}$$

and

$$Ra^* > 38A^{0.85}\kappa^{0.22}, \quad \text{for boundary layer flow.} \tag{22}$$

Equations (21) and (22) are expected to predict Ra^* within 10% of the critical Rayleigh numbers.

It is observed that the rate of increase of Nusselt number decreases as the radius ratio increases when the Rayleigh number is high (Fig. 8). This is not true for low Rayleigh numbers. Actually, for the pure conduction, the slope of the $\ln(Nu_i)$ vs $\ln(\kappa)$ curve increases with an increase in κ (see Fig. 8). As Ra^* is increased, this trend diminishes and finally in the boundary layer regime the slope of the curve near $\kappa = 1$ is the highest. There may be some critical combinations of Ra^* and A, for which the slope remains almost constant, e.g. $Ra^* = 50$ and $A = 2$ (Fig. 8).

As is clear the slope of the curve for $\ln(Nu_i)$ vs $\ln(\kappa)$ is not a constant with respect to the radius ratio (Fig. 8). The variation in the slope is high for low radius ratios ($\kappa < 5$) and is small for high values of κ. For $\kappa \geqslant 5$, the slope is almost uniform for high Rayleigh numbers, i.e. boundary layer flow regime. Based upon these observations and the conduction solution, two convenient ranges of the radius ratio can be selected, one, $\kappa < 5$, and the other, $\kappa \geqslant 5$. This is a somewhat similar behavior as observed for the aspect ratio dependence in the vertical cavity, i.e. $A \geqslant 2$ and $A < 2$.

Further, for any fixed Ra^*, if $\kappa \to \infty$, the Nusselt number approaches the conduction value. As can be seen in Fig. 8, the difference between the Nusselt numbers for $Ra^* = 100$, $A = 20$ and for $Ra^* = 0$ (conduction) reduces greatly as the radius ratio increases. The same behavior is demonstrated by all other lines for which $Ra^* = \text{const.}$, at least for low Rayleigh numbers (Fig. 8). This is mainly due to the fact that the larger the radius ratio, the higher the Rayleigh number required to establish the convective flows [equation (21)]. Havstad and Burns [19] have rightly

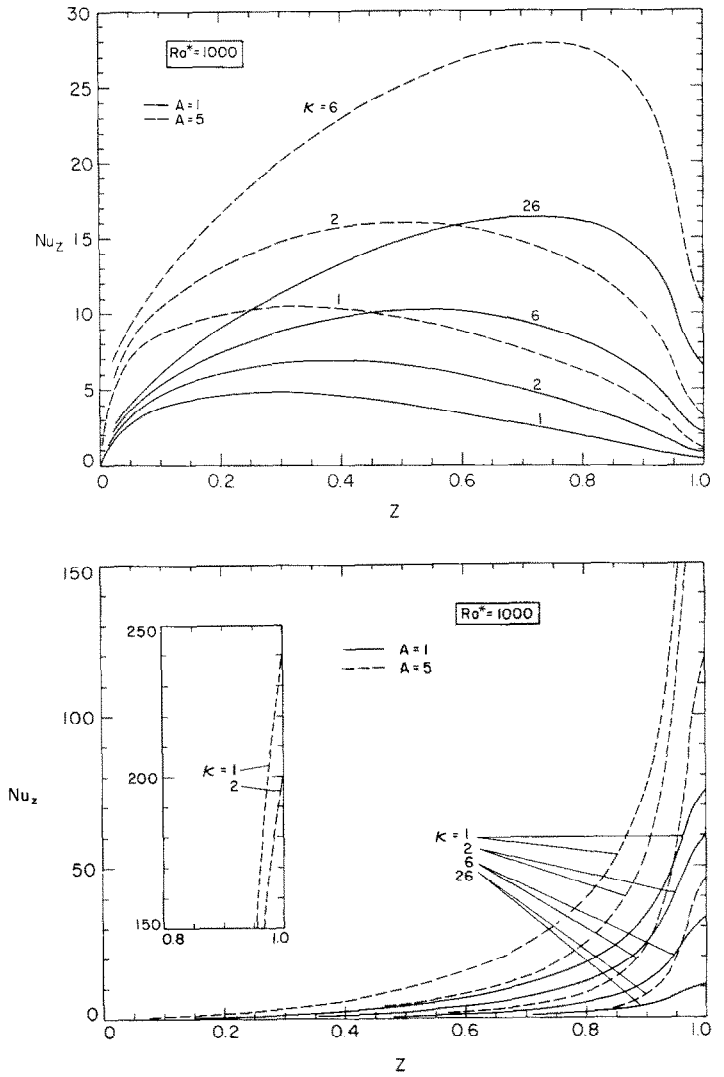

FIG. 5. Variation of local Nusselt number on vertical walls for $Ra^* = 1000$: (a) on the inner (heated) wall; and (b) on the outer (cold) wall (from top to bottom).

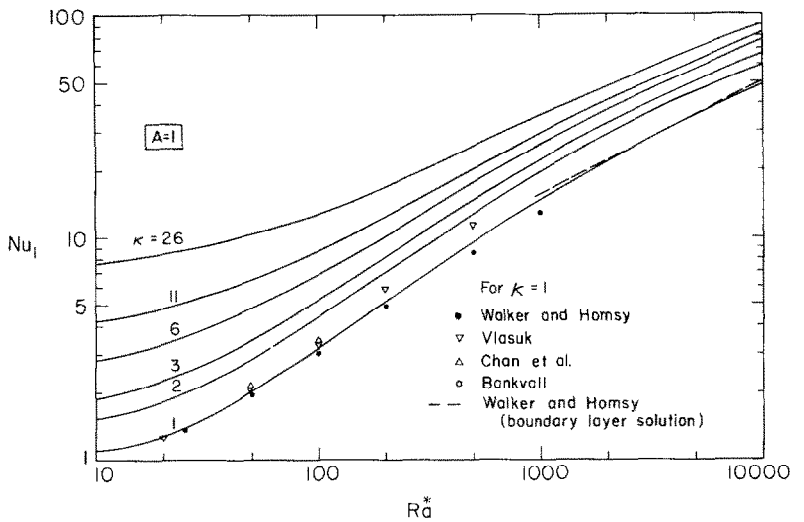

FIG. 6. Curvature effects on average Nusselt number, Nu_i, at the inner wall, for a square annulus.

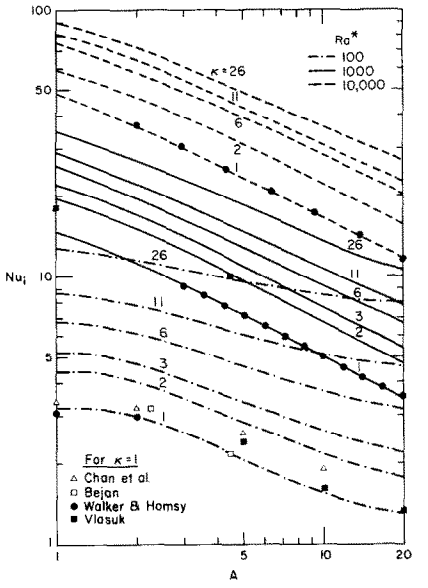

FIG. 7. Effect of radius ratio, κ, and aspect ratio, A, over average Nusselt number, Nu_i, for $Ra^* = 10^2$, 10^3 and 10^4.

assumed the conduction Nusselt number for $\eta = 0$ ($\kappa = \infty$) for any fixed L/r_o and $Ra^*_{r_o}$. It may be noted that the Rayleigh number, $Ra^*_{r_o}$, and the aspect ratio, L/r_o, defined by Havstad and Burns, approach the present value as the radius ratio increases, i.e. $Ra^*_{r_o} \to Ra^*$ and $L/r_o \to A$ as $\eta \to 0$.

For a tall cavity, an interesting conclusion can be derived for $\kappa \to \infty$. As discussed earlier, for high Rayleigh numbers, the slope of the ln (Nu_i) vs ln (κ) curve decreases as κ increases (see the $Ra^* = 10\,000$ line in Fig. 8). This indicates that the effect of the change in radius ratio on Nusselt number reduces with an increase in κ, provided the boundary layer flow is always maintained, i.e. for Ra^* greater than the critical Rayleigh number given by equation (22). Since for high radius ratios, the effective sink temperature for the

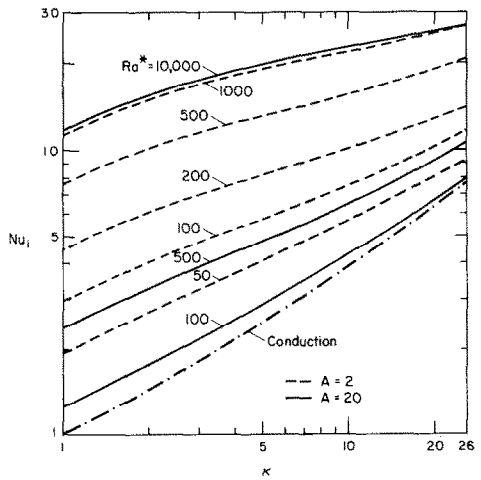

FIG. 8. Effects of radius ratio on the heat transfer rate for various Rayleigh numbers.

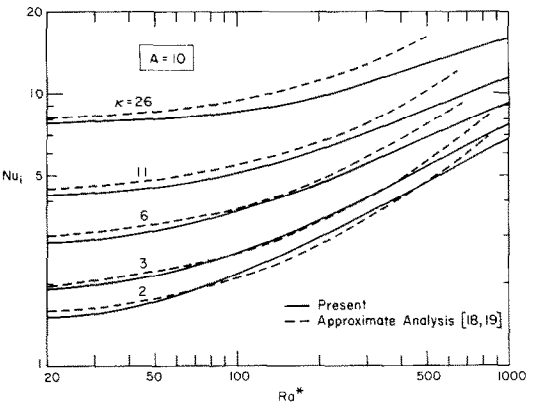

FIG. 9. Present numerical results compared with the results of the approximate analysis of Hickox and Gartling [18], and Havstad and Burns [19]. The constant C [equation (27)] is taken as 0.57 [19].

boundary layer on the inner wall is much closer to the outer wall temperature (Fig. 4), the Nusselt number in the present case should asymptotically approach the value obtained for a boundary layer on a heated vertical cylinder as $\kappa \to \infty$. For $Ra^* = 10\,000$, $A = 20$ and $\kappa = 26$, the Nusselt number obtained for a cylinder maintained at a temperature T_i and embedded in a saturated porous medium at T_o, is 27.39 (obtained from Minkowycz and Cheng [26]). The present value is 26.94, which differs by only 1.64%. As can be expected, this difference increases if A and/or κ is reduced. For $\kappa = 3$, the present value is 15% lower than that in the case of a cylinder, for the above values of Ra^* and A. Similarly, for $A = 1$, the Nusselt number for the annulus is 8.5% lower than that for the cylinder, for $Ra^* = 10\,000$ and $\kappa = 26$.

It is also observed that the lower the Rayleigh number the larger is the deviation from the cylinder solution. For $Ra^* = 1000$, the cylinder Nusselt number is 24% higher than the present value when $A = 20$ and $\kappa = 26$. In general, the cylinder solution will be higher than the annulus results. The reasons are; the sink temperature considered for the cylinder, T_0, is lower than that for the inner boundary layer in the case of the annulus, and the end effects are not present for the boundary layer on a cylinder. It may be noted that the appropriate Rayleigh number for the cylinder is Ra^*_L, a Rayleigh number based upon the height.

It is of interest to know how the heat transfer rate is affected by an increase in the radius ratio, once the Nusselt number for the present case is the same as that for the cylinder. Is there any critical radius ratio beyond which the Nusselt number will start decreasing for any fixed Ra^*? The present range of the radius ratio is not extensive enough to have a conclusive answer. It may be recalled that the Nusselt number approaches conduction value as $\kappa \to \infty$, at least for low Rayleigh numbers.

An important observation can be made for the effect of aspect ratio on Nusselt number. The general conclusion [5] that the Nusselt number always attains a maximum value somewhere between $A = 1$ and 2 for

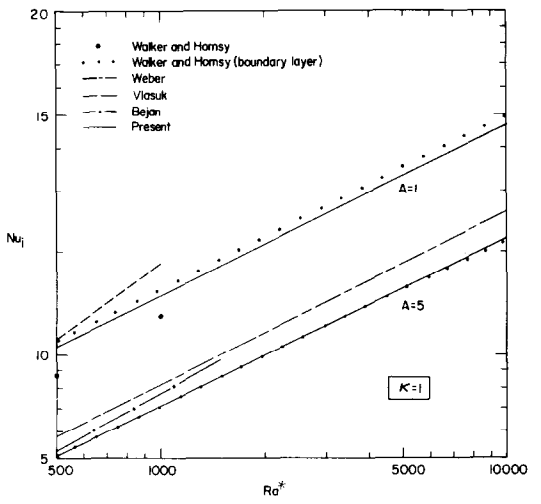

FIG. 10. Present correlations compared with previous results for vertical cavity, $\kappa = 1$, for $A = 1$ and 5.

the vertical cavity is not true. It is seen that as the Rayleigh number increases, the aspect ratio at which the Nusselt number is maximum shifts towards $A = 1$, and for high Rayleigh number this value of A is definitely below 1 (Fig. 7). A similar conclusion has also been reported by Havstad and Burns [19]. Any increase in curvature effects is found to boost up this trend (Fig. 7), and even at moderate Rayleigh numbers, the Nusselt number is maximum at $A < 1$ for high radius ratios.

4.4. *Correlations*

Based upon the heat transfer results, the following correlations are presented for the boundary layer regime.

For a square annulus, $A = 1$

$$Nu_i = 0.49 Ra^{*0.495}\, \kappa^{0.38}, \quad 1 \leqslant \kappa < 5, \tag{23}$$

and

$$Nu_i = 0.78 Ra^{*0.46}\, \kappa^{0.2}, \quad \kappa \geqslant 5. \tag{24}$$

For a tall annulus, $A \geqslant 2$

$$Nu_i = 0.47 Ra^{*0.51}\, A^{-0.49} \kappa^{0.38}, \quad 1 \leqslant \kappa < 5, \tag{25}$$

and

$$Nu_i = 0.74 Ra^{*0.47}\, A^{-0.46} \kappa^{0.22}, \quad \kappa \geqslant 5. \tag{26}$$

Equations (23) and (24) are valid for $Ra^* \geqslant 500$, and predict the Nusselt number to within 3% for $Ra^* \geqslant 10^3$, for the low radius ratio range, and within 4% for the high radius ratio range except when $Ra^* < 10^3, \kappa < 15$ and $Ra^* > 3000, \kappa > 25$. Similarly, heat transfer rates predicted by equations (25) and (26) are within 5% for $Ra^* \geqslant 500$, $\kappa < 5$ and $500 < Ra^* < 10^4$, $\kappa < 10$ compared to the numerical results. In all other cases the predicted values are within 10% of the computed ones. The deviation is a little larger for $Ra^* < 700$ and $\kappa > 10$.

The above deviations between the predicted and the numerical values are mainly due to the continuous change in the slope of the ln (Nu_i) vs ln (κ) curves, and the lower slope of the curve for high Rayleigh numbers and large radius ratios (approaching embedded cylinder solution). However, equations (23)–(26) present average slopes for two different radius ratio ranges, the basis for which has already been discussed.

4.5. *Comparison with previous results*

In Figs. 6 and 7, the present results for the vertical cavity, $\kappa = 1$, have been compared with some of the existing results. As can be seen, for $A = 1$ (Fig. 6) the values of Nusselt number agree with most of the results for low values of Ra^*; agree well with Walker and Homsy's results [12] for high Ra^*; and lies in between Vlasuk's [6] and Walker and Homsy's [12] results for moderate Ra^*. For the tall cavity (Fig. 7) the agreement with Walker and Homsy's boundary layer solution [12] is excellent. Compared to Vlasuk's work, the present values of the Nusselt numbers are 20–30% less for $Ra^* = 10^3$. At $Ra^* = 10^2$, the present results are in excellent agreement with some of the results of Chan *et al.* [5], Bejan [13], Walker and Homsy [12] and others. An encouraging fact is the agreement of the present results with previous work at high Rayleigh number, up to $Ra^* = 10^4$.

In Fig. 10, the predicted Nusselt numbers by equations (23) and (25) have been compared with the results of other investigators for the vertical cavity. As can be seen, the present results are in excellent agreement with Walker and Homsy's results [12], for the tall cavity. For a square cavity, equation (23) predicts results 5% lower than their boundary layer results, whereas for a tall cavity the prediction is up to 5% higher. The present values are 11–16% lower than Weber's results [10] for $A = 5$, whereas for the square cavity, they are quite close to Bejan's values [13], within 7%. The difference with Weber's results reduces as the aspect ratio increases (about 10% at $A = 20$).

For the tall vertical annulus, an approximate analysis has been presented by both Hickox and Gartling [18], and Havstad and Burns [19] following the work of Burns *et al.* [11] and Batchelor [20]. The expression for the Nusselt number obtained by them [18, 19], in a simplified form, is

$$\frac{Nu_i}{(Nu)_{\text{cond}}} = 1 + C \frac{Ra^*}{A} \times \left\{ \frac{\ln \eta}{2(1-\eta)^2} \left[\frac{\eta^2}{(1-\eta^2)} - \frac{1}{4} \frac{(1-\eta^2)}{(\ln \eta)^2} \right] \right\}. \tag{27}$$

Based upon their numerical results, Hickox and Gartling [18], and Havstad and Burns [19] have obtained the values for C as 0.585 and 0.57, respectively.

The Nusselt numbers obtained from equation (27) with $C = 0.57$ [19] are compared with the present numerical results in Fig. 9, for $A = 10$. As can be seen the two values are quite close to each other for low Rayleigh numbers and low radius ratios. For $\kappa = 2$, the difference is within 6% for Ra^* up to 700, whereas for $\kappa = 6$ this is true only up to $Ra^* \simeq 400$. This indicates

Table 1. Comparison of present values of average Nusselt number with the values obtained by Hickox and Gartling [18] for $Ra^* = 100$

	$A = 2$			$A = 4$			$A = 6$			$A = 8$		
κ	2	3	5	1.5	2	3	1.33	1.67	2.33	1.25	1.5	2
Hickox and Gartling [18]	4.190	4.741	5.590	2.879	3.216	3.750	2.277	2.506	2.886	1.951	2.117	2.409
Present results	4.048	4.738	5.716	2.751	3.123	3.692	2.172	2.412	2.806	1.862	2.033	2.327

that the approximate method [18, 19] yields reasonable results for the low Rayleigh numbers and small radius ratios. This is mainly a result of the assumptions made in the approximate analysis, i.e. $\partial u/\partial z$, $\partial^2 T/\partial z^2$ and $(\bar{V}\cdot\nabla T)$ are negligible; these are not valid for large radius ratios or high Ra^* (see streamline and isotherm contours). A similar disagreement has also been reported by Havstad and Burns [19] and Hickox and Gartling [18]. The numerical results of Havstad and Burns agree within 6% to the asymptotic solution for κ only up to 3.33 and $A > 2$. As already reported [18, 19], the agreement between the asymptotic and the numerical solutions improves as the aspect ratio increases. The present numerical result is 5.6% lower than the asymptotic solution for $Ra^* = 500$ and $A = 20$, whereas the difference is 8.4% for $Ra^* = 100$ and $A = 5$, when the radius ratio is 11.

The average Nusselt numbers obtained by Hickox and Gartling [18], by using a finite element method, have been compared with the present numerical values, for $Ra^* = 100$, in Table 1. The maximum difference between the two results is 4.8%. A similar agreement is observed for other Rayleigh numbers. In Table 2, the present Nusselt numbers are compared with the numerical results of Havstad and Burns [19] for selected values of Ra^*, A and κ. The maximum difference is up to 11.3%, but for most of their results, the difference is within 6%.

4.6. *Effects of aspect ratio*

Before closing, it is worthwhile to reconsider the correlations, reported by different investigators [4, 8, 10, 12] and the ones presented here. For a vertical cavity, equation (18) can be expressed in terms of Nusselt number and Rayleigh number based upon the cavity height, L, as

$$Nu_L = 0.47 Ra_L^{*0.51}, \quad A \geqslant 2. \tag{28}$$

This indicates that the Nusselt number is independent of aspect ratio for $A \geqslant 2$ if the boundary layer regime is maintained, i.e. the Rayleigh number is always greater than the critical value for the boundary layer flow [15]. A similar conclusion can be stated for the correlations given by Walker and Homsy [12]

$$Nu_L = (0.51 \pm 0.01) Ra_L^{*0.5}, \tag{29}$$

and, Weber [10]

$$Nu_L = 0.58 Ra_L^{*0.5}. \tag{30}$$

Thus, for any given height L, if the width D is increased, the heat transfer rate remains unchanged provided, by doing this, the aspect ratio is not reduced below two.

Now, consider some of the other correlations. The result of Bories and Combarnous's study [8] is

$$Nu_L = 0.245 Ra_L^{*0.625} A^{-0.022}, \tag{31}$$

whereas, the experimental work of Seki *et al.* [4] shows that

$$Nu_L = 0.627 Ra_L^{*0.473} Pr^{0.13} A^{0.001}. \tag{32}$$

Equation (32) predicts a Nusselt number 0.16% higher for $A = 25$, compared to that for $A = 5$. At this stage it is difficult to decide what should be the exponent for A, and whether it should be negative or positive. But based upon equations (28)–(32), it can be definitely concluded that the heat transfer coefficient is a very weak function of aspect ratio for the tall vertical cavity case (in the boundary layer regime).

For the vertical annulus, equations (25) and (26) transform to

$$(Nu_L)_i = 0.47 Ra_L^{*0.51} \kappa^{0.38}, \quad 1 \leqslant \kappa < 5, \tag{33}$$

and

$$(Nu_L)_i = 0.74 Ra_L^{*0.47} A^{0.03} \kappa^{0.22}, \quad \kappa \geqslant 5. \tag{34}$$

Again, in this case, it appears that the heat transfer rate is a very weak function of aspect ratio for $A \geqslant 2$. The same conclusion is not true with regard to the radius ratio. Clearly, the Nusselt number always increases as the radius ratio increases, and so does the heat transfer

Table 2. Present Nusselt numbers compared with numerical results of Havstad and Burns [19]

	$\kappa = 2$				$\kappa = 5$				$\kappa = 10$			
Ra^*	75	50	50	50	120	120	80	80	135	135	90	90
A	1	1	10	20	2.5	6.25	2.5	12.5	2.222	5.555	2.222	11.11
Havstad and Burns [19]	3.85	2.92	1.83	1.62	6.48	4.62	5.14	3.18	8.98	6.82	7.31	4.85
Present results	3.59	2.77	1.72	1.57	5.79	4.15	4.83	2.99	8.17	6.05	6.88	4.54

coefficient for any given height of the annulus. A similar conclusion with regard to radius ratio can be derived from the results of Havstad and Burns [19], and Hickox and Gartling [18]. It can, therefore, be concluded that any increase in the radius ratio results in an enhancement of the heat transfer rate for a vertical annulus of fixed height, if the inner radius r_i is either kept constant or increased.

5. CONCLUSION

Numerical results obtained for natural convection in a vertical annulus filled with a saturated porous medium indicate the following:

(1) Introduction of curvature effects completely disturbs the centro-symmetrical properties of the vertical cavity case and significantly influences the temperature and velocity fields.

(2) A large percentage of heat is rejected in a very small distance from the top edge of the cooled wall. The higher the aspect ratios and/or lower the radius ratios, the higher is the heat transfer rate in the top portion.

(3) As the radius ratio is increased the conduction and asymptotic flow regimes get extended (in terms of Rayleigh number). An increase in κ extends the conduction regime much more compared to the extension of the asymptotic regime. The critical Rayleigh numbers to delimit the flow regimes are given by equations (21) and (22).

(4) The growth of boundary layers is affected by a change in the radius ratio and the start of the boundary layer regime is delayed as κ is increased.

(5) The slope of the $\ln(Nu_i)$ vs $\ln(\kappa)$ curve changes as the radius ratio increases, the highest slope being at $\kappa = 1$. The change in the slope is very small for $\kappa > 5$ at high Rayleigh numbers. Based upon the conduction solution and the results for $Ra^* > 0$, two convenient ranges for the radius ratio can be selected for practical purposes, one $\kappa < 5$ and the other, $\kappa \geqslant 5$.

(6) The average Nusselt number on the inner wall always increases as the radius ratio increases, and indicates that the heat transfer coefficient increases with an increase in the curvature effects.

(7) The sink temperature for the boundary layer on the inner wall decreases with an increase in the radius ratio. This brings the annulus results close to the heat transfer results for a heated vertical cylinder embedded in a saturated porous media, provided the Rayleigh number is high enough to maintain the boundary layer flow. Hence, for a tall annulus with large radius ratio, the cylinder solution can be used within a reasonable accuracy, provided the Rayleigh number is high enough to maintain the boundary layer flow.

(8) The aspect ratio at which the Nusselt number is maximum strongly depends on the Rayleigh number and the radius ratio. The higher the Rayleigh number and/or radius ratio, the lower is the value of A for the maximum Nu_i.

(9) In the boundary layer regime, the heat transfer coefficient is a very weak function of the aspect ratio, for $A \geqslant 2$, for both the vertical cavity and the vertical annulus.

(10) For two different ranges of radius ratio, $1 \leqslant \kappa < 5$ and $\kappa \geqslant 5$, four correlations, equations (23)–(26), are required to predict the heat transfer rates, i.e. two for the square annulus and two for the tall annulus. These equations predict average Nusselt number for the boundary layer flow regime, and are based upon the average slopes of the $\ln(Nu_i)$ vs $\ln(\kappa)$ curves for the present range of Ra^*, A and κ.

However, experimental studies are required to verify the present results and the form of these correlations.

REFERENCES

1. M. A. Combarnous and S. A. Bories, Hydrothermal convection in saturated porous media, *Adv. Hydroscience* **10**, 231–307 (1975).
2. P. Cheng, Heat transfer in geothermal systems, *Adv. Heat Transfer* **14**, 1–105 (1978).
3. M. Combarnous, Natural convection in porous media and geothermal systems, 6th Int. Heat Transfer Conf., Toronto, Vol. 6, pp. 45–59 (1978).
4. N. Seki, S. Fukusako and H. Inaba, Heat transfer in a confined rectangular cavity packed with porous media, *Int. J. Heat Mass Transfer* **21**, 985–989 (1978).
5. B. K. C. Chan, C. M. Ivey and J. M. Barry, Natural convection in enclosed porous media with rectangular boundaries, *J. Heat Transfer* **2**, 21–27 (1970).
6. M. P. Vlasuk, Transfert de chaleur par convection dans une couche poreuse, *Proc. 4th All-union Heat Mass Transfer Conf.*, Minsk (1972). (Referred by Combarnous and Bories [1].)
7. P. H. Holst and K. Aziz, A theoretical and experimental study of natural convection in a confined porous medium, *Can. J. Chem. Engng* **50**, 232–241 (1972).
8. S. A. Bories and M. A. Combarnous, Natural convection in a sloping porous layer, *J. Fluid Mech.* **57**, 63–93 (1973).
9. C. G. Bankvall, Natural convection in vertical permeable space, *Warme- und Stoffubertragung* **7**, 22–30 (1974).
10. J. E. Weber, The boundary layer regime for convection in a vertical porous layer, *Int. J. Heat Mass Transfer* **20**, 569–573 (1975).
11. P. J. Burns, L. C. Chow and C. L. Tien, Convection in a vertical slot filled with porous insulation, *Int. J. Heat Mass Transfer* **20**, 919–926 (1976).
12. K. L. Walker and G. M. Homsy, Convection in a porous cavity, *J. Fluid Mech.* **97**, 449–474 (1978).
13. A. Bejan, On the boundary layer regime in a vertical enclosure filled with a porous medium, *Lett. Heat Mass Transfer* **6**, 93–102 (1979).
14. P. G. Simpkins and P. A. Blythe, Convection in a porous layer, *Int. J. Heat Mass Transfer* **23**, 881–887 (1980).
15. V. Prasad and F. A. Kulacki, Convective heat transfer in a rectangular porous cavity—effect of aspect ratio on flow structure and heat transfer, *J. Heat Transfer* (in press). Also presented at the 21st National Neat Transfer Conf., Seattle, ASME Paper No. 83-HT-66 (1983).
16. V. Prasad, Natural convection in porous media—an experimental and numerical study for vertical annular and rectangular enclosures, Ph.D. dissertation, University of Delaware, Newark, Delaware (1983).
17. V. Prasad and F. A. Kulacki, Natural convection in a rectangular porous cavity with constant heat flux on one vertical wall, *J. Heat Transfer* (in press). Also in *ASME HTD* (edited by J. V. Beck and L. S. Yao), Vol. 22, pp. 35–41. Winter Annual Meeting, Phoenix (1982).
18. C. E. Hickox and D. K. Gartling, A numerical study of

natural convection in a vertical, annular, porous layer, 21st National Heat Transfer Conf., ASME, Paper No. 82-HT-68 (1982).
19. M. A. Havstad and P. J. Burns, Convective heat transfer in vertical cylindrical annuli filled with a porous medim, *Int. J. Heat Mass Transfer* **25,** 1755–1766 (1982).
20. G. K. Batchelor, Heat transfer by free convection across a closed cavity between vertical boundaries at different temperatures, *Q. Jl Appl. Math.* **12,** 209–233 (1954).
21. A. D. Gosman, W. M. Pun, A. K. Runchal, D. B. Spalding and M. Wolfshtein, *Heat and Mass Transfer in Recirculating Flows.* Academic Press, New York (1969).
22. P. J. Roache, *Computational Fluid Dynamics.* Hermosa, Albuquerque, New Mexico (1976).
23. G. de Vahl Davis and R. W. Thomas, Natural convection between concentric vertical cylinders, *Physics Fluids* Supplement II, 198–207 (1969).
24. R. W. Thomas and G. de Vahl Davis, Natural convection in annular and rectangular cavity—a numerical study, *Proc. 4th Int. Heat Transfer Conf.*, Paris, Vol. 4, NC 2.4, Elsevier, Amsterdam (1970).
25. Y. Lee, S. A. Korpela and R. N. Horne, Structure of multicellular natural convection in a tall vertical annulus, 7th Int. Heat Transfer Conf., Munich (1982).
26. W. J. Minkowycz and P. Cheng, Free convection about a vertical cylinder embedded in a porous medium, *Int. J. Heat Mass Transfer* **19,** 805–813 (1976).

CONVECTION NATURELLE DANS UN ESPACE ANNULAIRE POREUX VERTICAL

Résumé—Des études numériques sont faites pour la convection naturelle permanente dans un espace annulaire vertical rempli d'un matériau poreux saturé et dont les parois verticales sont à températures constantes, les parois horizontales étant adiabatiques. Des effets de courbures sur les champs de température et de vitesse sont significatifs et ils perturbent complètement la nature centro-symétrique trouvée dans le cas de la cavité verticale. Des vitesses convectives sont plus grandes dans la moitié supérieure que dans la moitié inférieure de l'espace, et le flux thermique local est plus élevé près de l'extrémité supérieure de la paroi froide. Le nombre de Nusselt moyen croît toujours quand le rapport des rayons κ augmente, tandis que la vitesse d'accroissement diminue avec l'augmentation des effets de courbure, particulièrement aux nombres de Rayleigh Ra^* élevés. Dans le cas d'un anneau étroit, le flux thermique dans l'écoulement de couche limite approche celui pour un cylindre noyé dans un milieu poreux quand κ augmente. Les critères de nombre de Rayleigh pour différents régimes d'écoulement sont obtenus, et le nombre de Nusselt moyen est exprimé par une relation de la forme $Nu = \text{Cte}\ Ra^{*m} A^n \kappa^p$, où A est rapport de forme (hauteur/largeur). Dans le régime de couche limite, le flux thermique pour une cavité de l'anneau de hauteur fixée est une fonction très faible du rapport de forme.

NATÜRLICHE KONVEKTION IN VERTIKALEN PORÖSEN RINGRÄUMEN

Zusammenfassung—Numerische Untersuchungen werden vorgestellt über die stationäre natürliche Konvektion in vertikalen Ringräumen, die mit einem gesättigten porösen Stoff gefüllt sind und deren vertikale Wände auf einer konstanten Temperatur gehalten werden. Die horizontalen Wände sind isoliert. Der Einfluß der Krümmung auf das Temperatur- und Geschwindigkeits-Feld ist von besonderer Bedeutung, er zerstört die Zentralsymmetrie, die im vertikalen Hohlraum zu beobachten ist. Die Strömungsgeschwindigkeiten sind in der oberen Hälfte des Ringraumes größer als in der unteren Hälfte, der örtliche Wärmeübergang ist am oberen Ende der kalten Wand wesentlich größer. Die mittlere Nusselt-Zahl nimmt stets mit dem Radienverhältnis κ zu, obwohl sich die Zuwachsrate mit zunehmendem Krümmungs-Einfluß verringert, besonders bei hohen Rayleigh-Zahlen, Ra^*. Im Fall eines hohen Ringraumes erreicht der Wärmeübergang im Bereich der Grenzschichtströmung die Werte für einen Zylinder, der in einem porösen Medium eingebettet ist, weil nämlich κ ansteigt. Für verschiedene Strömungsbereiche ergibt sich ein Rayleigh-Zahl-Kriterium. Die mittlere Nusselt-Zahl wird durch eine Beziehung der Form $Nu = \text{Konstante}\ Ra^{*m} A^n \kappa^p$ korreliert, wobei A das Längenverhältnis (Höhe zu Spaltweite) ist. Im Bereich der Grenzschichtströmung hängt der Wärmeübergang in einem großen Hohlraum oder Ringraum von fester Höhe nur wenig vom Längenverhältnis ab.

ЕСТЕСТВЕННАЯ КОНВЕКЦИЯ В ВЕРТИКАЛЬНОМ ПОРИСТОМ КОЛЬЦЕОБРАЗНОМ СЛОЕ

Аннотация—Представлены численные исследования установившейся свободной конвекции в вертикальном кольцеобразном слое, заполненном насыщенной пористой средой, вертикальные стенки которого имеют постоянную температуру, а горизонтальные – изолированы. Влияние кривизны на поля температуры и скорости существенно, так как полностью нарушает симметричную картину, обнаруженную в случае вертикальной полости. В верхней части кольцеобразного слоя конвективные скорости выше, чем в нижней, а локальная скорость теплопереноса намного больше у верхней кромки холодной стенки. Среднее число Нуссельта всегда растет как отношение радиусов κ, хотя скорость роста уменьшается с увеличением влияния кривизны, в частности, при больших числах Рэлея Ra^*. В случае высокого кольцеобразного слоя и с ростом κ скорость теплопередачи в режиме течения пограничного слоя приближается к скорости для случая цилиндра, помещенного в пористую среду. Получены критерии числа Рэлея для различных режимов течения, а среднее число Нуссельта определяется соотношением типа $Nu = \text{const}.\ Ra^{*m}\ A^n \kappa^p$, где A – относительное удлинение (высота к толщине стенки). В режиме пограничного слоя скорость теплопередачи для высокой замкнутой полости или для кольцеобразного слоя ограниченной высоты является очень слабой функцией относительного удлинения.